ACS APPLIED MATERIALS & INTERFACES

Forum Article

www.acsami.org

Ultrathin Body Poly(3-hexylthiophene) Transistors with Improved Short-Channel Performance

Chenchen Wang,[†] Jonathan Rivnay,[‡] Scott Himmelberger,[‡] Kiarash Vakhshouri,[§] Michael F. Toney,[⊥] Enrique D. Gomez,[§] and Alberto Salleo*[,‡]

[†]Department of Applied Physics and [‡]Department of Materials Science and Engineering, Stanford University, Stanford, California 94305, United States

[§]Department of Chemical Engineering, The Pennsylvania State University, University Park, Pennsylvania 16802, United States

[⊥]Stanford Synchrotron Radiation Lightsource, SLAC National Accelerator Laboratory, Menlo Park, California, United States

ABSTRACT: The microstructure and charge transport properties of binary blends of regioregular (rr) and regiorandom (RRa) poly(3-hexylthiophene) (P3HT) are investigated. X-ray diffraction of the blended films is consistent with a vertically separated structure, with rr-P3HT preferentially crystallizing at the semiconductor/dielectric interface. Thin film transistors made with these blended films preserve high field effect mobility with rr-P3HTcontent as low as 5.6%. In these dilute blends, we estimate that the thickness of rr-P3HT in the channel is only a few nanometers. Significantly, as a result of such an ultrathin active layer at the interface, short channel effects due to bulk currents are eliminated, suggesting a new route to fabricate high-performance, short-channel, and reliable organic electronic devices.

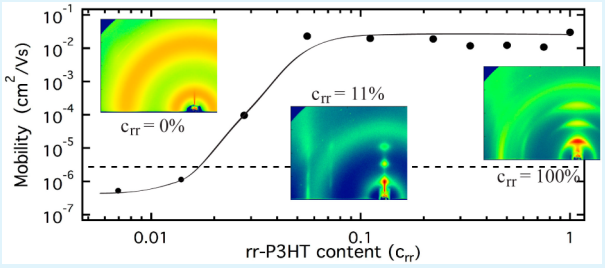

KEYWORDS: *conjugated polymers, thin-film-transistors, interface, charge transport, organic electronics*

INTRODUCTION

Organic semiconductors have attracted broad interest in the past few decades because of their potential applications in organic light-emitting diodes (OLEDs), low-cost flexible circuits, biosensors, and photovoltaics.[1,2] Poly(3-hexylthiophene) (P3HT) is one the most widely studied high-performance semiconducting polymers, providing good performance in solar cells and transistors. When first reported, the mobility of P3HT was low, on the order of 1×10^{-5} to 1×10^{-4} $cm^2/(V\ s)$.[3] Carrier mobility increased when it was realized that the semicrystalline microstructure afforded by control of the polymer regioregularity was beneficial for charge transport.[4−6] Currently, a field-effect mobility on the order of 0.1 $cm^2/(V\ s)$ is commonplace in high regioregularity P3HT.[7−9] Many new high-performance semiconducting polymers also exhibit a semicrystalline microstructure, and therefore the wealth of experimental data accumulated on P3HT over the years make it a widespread model system to study transport in other semiconducting, semicrystalline polymers.

Reducing costs is one of the main rationales for investigating solution-processable materials, such as semiconducting polymers. Notably, in devices such as thin film transistors, the active semiconductor layer is a few nanometers thick, which in principle leaves room to drastically reduced materials utilization. Following this realization, composites of P3HT and commodity polymers (e.g., polyethylene or polystyrene) were recently described, where the carrier mobility of neat P3HT was preserved at concentrations as low as 3 wt %.[10−12] These polymer blends thus combined a lower active material utilization with the improved processability of the high molecular-weight commodity polymers. The high field-effect mobility of the blends is due to phase separation, whereby the minority component (P3HT) segregates at the substrate surface, forming a thin active layer while the remaining material does not play any active role in the electronic device. Surface energy can also be used to generate patterns in the lateral direction to self-assemble arrays of isolated devices by taking advantage of its effect on phase segregation in polymer blends.[13] Most of these phase separation processes however require annealing to guarantee the formation of a continuous semiconducting film at the substrate surface. In this work, we report the use of regioregular(rr)/regiorandom(RRa) polythiophene blends, where the regiorandom fraction plays the role of an insulator. These blends phase-separate readily upon spin-coating without the need for thermal annealing, with the regioregular polythiophene preferentially segregating at the substrate surface. Such a facile phase separation process allows the formation of ultrathin semiconducting layers in contact with the gate dielectric. As a result, the materials utilization of the

Special Issue: Forum on Advancing Technology with Organic and Polymer Transistors

Received: November 15, 2012
Accepted: February 4, 2013
Published: February 21, 2013

   dx.doi.org/10.1021/am3027103 | *ACS Appl. Mater. Interfaces* 2013, 5, 2342−2346

high-value polymer is kept to a minimum since blends with less than 10% loading of the regioregular component perform as well as the neat regioregular polymer. Furthermore, we investigate the microstructure of rr-P3HT/RRa-P3HT blend films by X-ray diffraction, and we correlate this to the charge transport properties of the films. We conclude that these blends form ultrathin body TFTs, which do not suffer from the short-channel effects commonly observed in organic TFTs with channel lengths shorter than 10 μm,[14,15] thereby helping enable the downscaling of this technology.

RESULTS AND DISCUSSION

The starting solution is prepared by blending 1 wt % rr-P3HT and 1 wt % RRa-P3HT in 1,2-dichlorobenzene (DCB). The rr-P3HT used in most of our experiments reported here had regioregularity >98%, and a molecular weight (M_w) of 108 kDa. In one series of experiments, a low M_w polymer (22−25 kDa) was used. Devices were fabricated in the standard bottom-gate, bottom-contact configuration in a glovebox. The total thickness of all P3HT films was around 70 nm, with a variation of less than 7%. Finished devices were transferred in air to a vacuum probe station for electrical characterization. Pure low M_w rr-P3HT, high M_w rr-P3HT, and RRa-P3HT polymer transistors exhibited mobilities (measured in the saturation regime) of 5.7 × 10^{-2}, 4.2 × 10^{-2}, and 2.7 × 10^{-6} cm^2 V^{-1} s^{-1} respectively, consistent with literature reports.[3,16,17]

Mobilities from TFTs fabricated with different high M_w rr-P3HT concentrations (in a RRa-P3HT matrix), c_{rr}, measured as wt % are shown in Figure 1. For c_{rr} above 5.6 wt %, the mobility

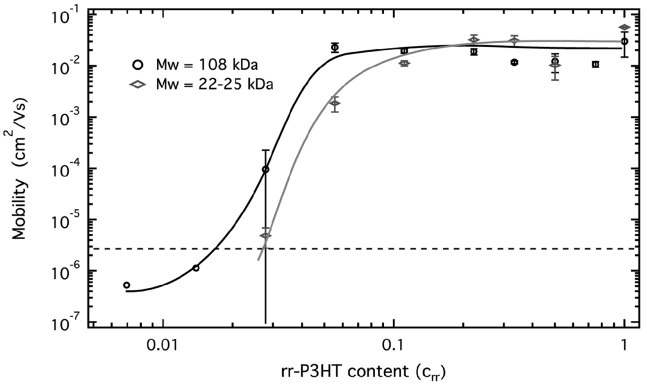

Figure 1. Field-effect mobility as a function of rr-P3HT content (c_{rr}), from devices with channel length of 20 and 50 μm. The dashed line is the mobility in neat RRa-P3HT film. The larger error bar in the high M_w blend at c_{rr} = 2.8 wt % is caused by the strong channel-length dependence of mobility, as described in the text.

of the TFTs made with the blends remains high and comparable to that of pure rr-P3HT. A rapid decrease in mobility is observed when c_{rr} drops below 5.6 wt %. At c_{rr} < 2.8 wt %, carrier mobility is 1 × 10^{-6} cm^2/(V s), close to the mobility we measure in pure RRa-P3HT. For blends made with both low M_w and high M_w rr-P3HT, the concentration threshold below which mobility decreases rapidly is nearly identical (2.8% and 5.6%, respectively) in spite of the large difference (~factor of 5) in molecular weight. This result suggests that the high mobility is not determined by the formation of a percolation path of rr-P3HT chains through the bulk of the RRa matrix, as in this case a strong polymer-length dependence of the concentration threshold where mobility decreases would be expected. The concentration threshold may however depend on total film thickness, controlled by the initial solution concentration. We did not explore such an effect in this work. We hypothesize that phase separation with the formation of a thin rr-P3HT layer at the substrate surface is the more likely cause for the high performance in TFTs of nominally dilute blends.

X-ray diffraction was used to characterize the rr-P3HT/RRa-P3HT blended films in order to investigate the presence of a semicrystalline rr-P3HT layer at the substrate surface. The two-dimensional grazing incidence X-ray diffraction (2D-GIXD) patterns show that neat RRa-P3HT is amorphous (Figure 2a), displaying diffuse halos common for amorphous macromolecular materials at $q \approx 0.2-0.5$ Å^{-1} and $q \approx 1.2-1.7$ Å^{-1}. Neat rr-P3HT on the other hand displays the typical (100), (200) and (300) lamellar peaks along q_z as well as the (020) peak associated with π-stacking at 1.7 Å^{-1} in q_{xy} (Figure 2b). Diffraction from a rr-P3HT/RRa-P3HT blend with c_{rr} = 11.1 wt % (Figure 2c) displays both features from the regioregular phase (peaks) and from the regiorandom phase (halo). Moreover, the mixed index peaks, which are usually observed in ultrathin or well-textured films,[18] are relatively more prominent in the blends with low regioregular content, than in the neat rr-P3HT film, suggesting that rr-P3HT crystallites have better ordering in the blends. Also, the arcing associated with (h00) peaks decreases as the regioregular content decreases, showing that there is an increase in edge-on texture of the crystallites as the regioregular fraction is decreased.

To be more quantitative, we combined the data from 2D-GIXD, 2D-Local Specular curves, and high-resolution rocking curves, and constructed pole figures (normalized by both film thicknesses and rr-P3HT content) of the (200) Bragg reflection,[19−21] as shown in Figure 2d. Pole figures describe the orientation distribution of crystallites as a function of polar angle and allow us to compare quantitatively the orientation and the degree of crystallinity of different blend films. Diffraction at a polar angle χ = 0° comes from crystallites with perfect edge-on texture, whereas χ = 90° corresponds to crystallites with face-on texture. The integral breadth of the pole figure, which is defined as the ratio of peak area to peak maximum, is very similar for all films with c_{rr} > 50 wt %, while differences arise at lower concentrations. At c_{rr} < 50 wt %, when rr-P3HT content decreases, the integral breadth decreases monotonically (Figure 3a) reaching a remarkable minimum of 2−3° at a c_{rr} of 5 wt %. Hence, as c_{rr} decreases, the texture of the crystallites acquires a more pronounced edge-on character, which is likely beneficial for in-plane charge transport.[22] It is worthwhile to note that the same trend of breadth reduction is observed in neat rr-P3HT films as a function of film thickness,[18] which suggests that the rr-P3HT in the blend phase separates into a film of decreasing thickness as its concentration is reduced. The narrowing of the pole figures of rr-P3HT/RRa-P3HT blend films suggests that a thin layer of crystalline rr-P3HT forms at the substrate surface, which provides a natural edge-on orientation preference for P3HT. Indeed, if rr-P3HT crystallites nucleated randomly within the RRa-P3HT matrix, one would expect that as the volume fraction of rr-P3HT decreases, the crystallites take on a more powder-like orientation distribution. Furthermore, the high carrier mobility of dilute blend films strongly suggests that there is a thin layer of crystalline rr-P3HT at the substrate surface. The diffraction signal from perfectly oriented crystallites at the interface,[23] however, was not sufficiently strong to directly

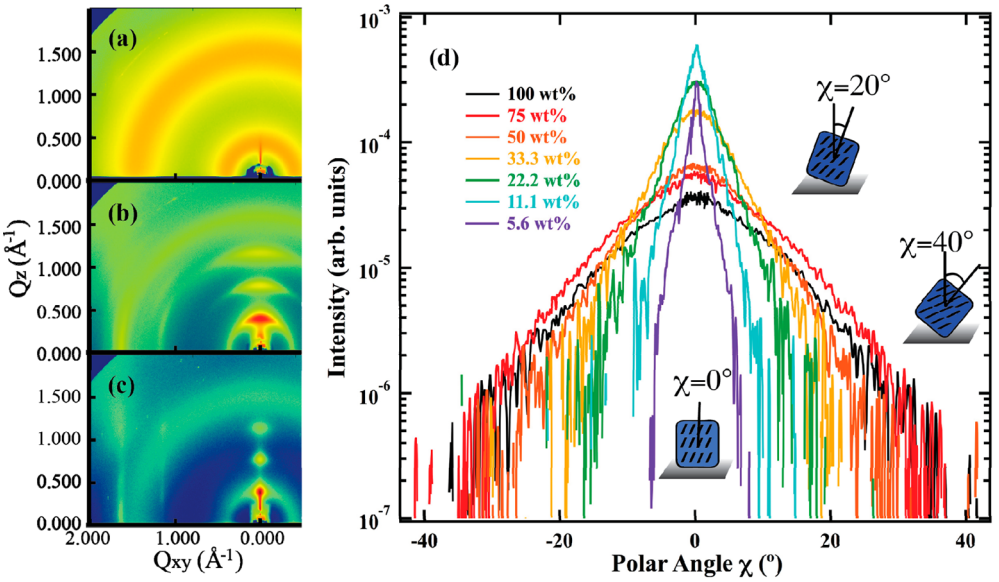

Figure 2. 2D-GIXD patterns of (a) RRa-P3HT, (b) rr-P3HT, and (c) rr-P3HT/RRa-P3HT blend film at c_{rr} = 11.1 wt %; (d) complete pole figures (normalized by both film thicknesses and rr-P3HT content) of the (200) Bragg reflection of rr-P3HT/RRa-P3HT blend films with different rr-P3HT contents c_{rr}.

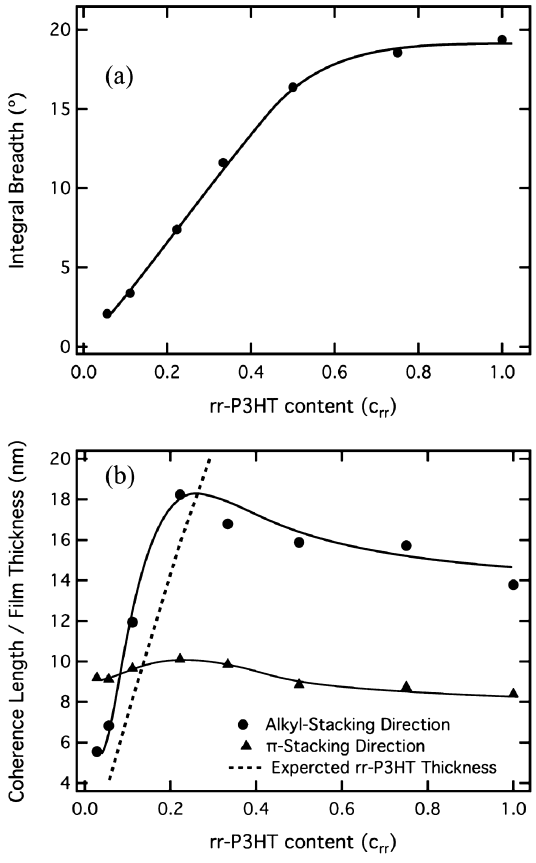

Figure 3. (a) Integral breadth extracted from the pole figures, (b) crystallite size in the alkyl stacking direction (circles) as well as coherence length in the $\pi\pi$ stacking direction (triangles), and expected film thickness if rr-P3HT wet the whole surface (dashed line), as a function of rr-P3HT content.

confirm the existence of an interface crystalline layer using XRD. We postulate that a sufficient density of crystallites in the blend films nucleate at or near the dielectric surface to participate in efficient charge transport. At c_{rr} < 11.1 wt % on the other hand, crystallization is hindered as the pole figure signal (and relative degree of crystallinity) decreases sharply.

We also estimate the crystalline coherence length in the lamellar direction (along the substrate normal) and the coherence length in the π-stacking direction (in the plane of the substrate) (Figure 3b), using the method of integral breadths[24] and Scherrer's equation,[25] respectively. The coherence length along the π-stacking direction does not significantly depend on rr-P3HT content, suggesting that blending does not affect the ability of the polythiophene chains to stack cofacially. In the lamellar direction the coherence length is essentially equivalent to the crystallite size.[26] Compared with neat rr-P3HT (13.8 nm), the slight increase (15.7−18.2 nm) in crystallite size along the alkyl chain stacking direction (100) at $c_{rr} \geq$ 22.2 wt % provides additional evidence of improved crystallization upon blending. When c_{rr} is smaller than 22.2 wt %, the coherence length decreases nearly linearly with decreasing rr-P3HT content. This decrease suggests that the crystalline P3HT fraction at the substrate surface is one crystallite thick: as the concentration of rr-P3HT decreases, so does the crystallite thickness. Further analysis of the diffraction data allows us to determine the driving force for phase separation. To this end, we compare in Figure 3b the crystallite thickness to the expected thickness of the rr-P3HT film if all the regioregular material was deposited at the substrate surface (dashed line), which is an upper bound as it assumes that no rr-P3HT is located at the film/air interface or dissolved in the RRa-P3HT bulk. When the rr-P3HT content is low (c_{rr} < 22.2 wt %), the observed crystallite thickness is larger than the maximum expected rr-P3HT film thickness. It should be added that the estimated crystallite thickness here is the average thickness of all crystallites inside the film. There most likely exist a number of smaller crystallites at the interface that can form conducting pathways for charge transport, together with the larger crystallites; therefore, it does not necessarily mean that the rr-P3HT coverage drops abruptly at 22.2 wt %. However, this simple estimate suggests that as the rr-P3HT concentration is reduced, there is an accumulation of polymer

dx.doi.org/10.1021/am3027103 | ACS Appl. Mater. Interfaces 2013, 5, 2342−2346

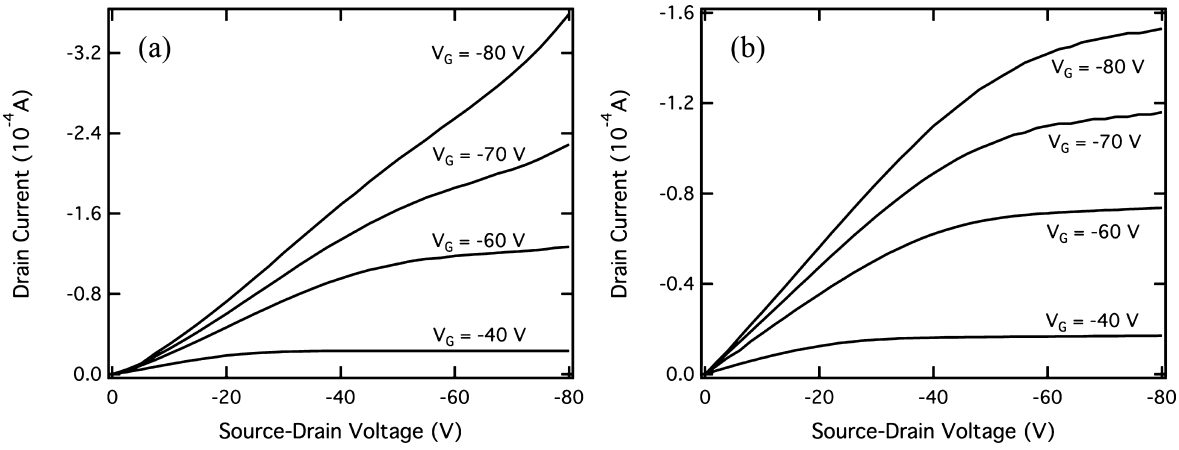

Figure 4. Output curves (I_D–V_D) of 5 μm-length channel TFTs made with (a) neat rr-P3HT and (b) a rr-P3HT/RRa-P3HT (high M_w) blend having c_{rr} = 11.1 wt %.

Table 1. Saturation Mobility of TFTs Made with a rr-P3HT/RRa-P3HT Blend at c_{rr} = 2.8 wt % as a Function of Channel Length

	channel length			
	5 μm	10 μm	20 μm	50 μm
mobility ($cm^2/(V\ s)$)	6.97×10^{-4}	5.02×10^{-4}	1.94×10^{-4}	4.39×10^{-6}

in the crystallites that have a large enough lamellar thickness that there is an eventually disappearance of percolation paths in the bottom layer of rr-P3HT. This would cause a rapid mobility decrease. It thus appears that crystallization of rr-P3HT rather than surface energy is the dominating driving force for phase separation since the polymer tends to form isolated crystallites rather than a continuous wetting layer. This is also confirmed by the fact, that on a similar but less hydrophobic surface (OTS treated briefly with UV ozone), phase separation with a similar concentration threshold was observed (data not shown). Nevertheless, crystallites grow preferentially at the substrate surface rather than inside the film because heterogeneous nucleation is always favored, leading to the observed microstructure.

The microstructure developed by phase-separation of the rr-P3HT/RRa-P3HT blends spontaneously produces ultrathin body TFTs at the lowest rr-P3HT concentration where an electrically continuous rr-P3HT film can form at the dielectric surface. It has been reported that in OFETs with channel lengths shorter than 10 μm, output curves (I_D–V_D) show a lack of current saturation. This phenomenon is commonly referred to as the short channel effect. The short channel effect is attributed to parasitic bulk currents in deep saturation due to the strong field at the drain electrode as well as electron (hole) injection from the drain electrode in hole (electron) channel devices.[14,15] Hence, the elimination of the semiconducting bulk should eliminate the short channel effect. In order to investigate this hypothesis, the characteristics of OFETs made with different blend compositions and having different channel lengths from 5 to 50 μm were measured. The short channel effect was observed in devices made with neat rr-P3HT having channel lengths of 5 and 10 μm (Figure 4a): the output curves do not saturate at high V_D, and the square law no longer holds. As a comparison, in the 11.1 wt % rr-P3HT device with 5 μm channel, short-channel effects disappear and the current saturates well at high drain voltage (Figure 4b). Generally speaking, for the blend films with different c_{rr}, the short channel effects become systematically less pronounced as c_{rr} decreases. The elimination of short-channel effects in devices with low rr-P3HT content suggests a reduction of parasitic currents through the bulk of the film near the drain contact. Because RRa-P3HT is essentially insulating, the microstructure obtained by phase separation precisely suppresses such bulk parasitic currents. Indeed, the ultrathin rr-P3HT layer is located at the gate surface and is therefore subject to the strong electrostatic control by the gate voltage. The RRa-P3HT overlayer on the other hand is not conducting and therefore cannot support sizable parasitic currents. As a result, the layered microstructure we observe in rr-P3HT/RRa-P3HT blends suppresses short-channel effects when the rr-P3HT layer is thin enough, that is at low c_{rr}.

Finally, mobility measurements also support the hypothesis of the presence of a discontinuous rr-P3HT film at the substrate surface when the rr-P3HT content is low (c_{rr} = 2.8 wt %), which is when the mobility drops (Figure 1). At this rr-P3HT concentration, the charge transport properties of OFETs are strongly dependent on channel lengths (Table 1). The mobility in these devices decreases systematically as the channel is made longer, and in particular a sharp decrease is noticed when the channel length increases from 20 to 50 μm, where the mobility is on the order of 1×10^{-6} $cm^2/(V\ s)$. These results suggest that at low rr-P3HT concentrations, discontinuities in rr-P3HT coverage occur at the few-micrometer length scale, such that transport pathways through high-mobility material still exist in devices having channel lengths commensurate with this length scale. The number of transport pathways decreases as the channel length increases. Therefore, in devices where the channel length is much larger than the length scale of the rr-P3HT discontinuities (e.g., 50 μm), charges must travel through the RRa-P3HT regions, which will impart overall low mobilities to the OTFTs.

CONCLUSION

In conclusion, films spin-cast from rr-P3HT/RRa-P3HT blends display charge transport properties comparable to those of neat rr-P3HT, even at rr-P3HT concentrations as low at 5.6%. X-ray

characterization of the films shows that the polymer blend undergoes vertical phase separation with the deposition of a rr-P3HT layer at the dielectric surface. Because RRa-P3HT is essentially insulating, at low rr-P3HT concentrations phase separation naturally leads to the formation of an ultrathin body TFT where the semiconductor thickness is merely a few nanometers. Such thin-body TFT exhibits good device characteristics down to channel lengths of 5 μm, where short channel effects always lead to strongly nonideal characteristics in neat P3HT transistors. Hence the use of these blends may allow the successful scale down of OTFTs to increase operating frequency and drive current.

AUTHOR INFORMATION

Corresponding Author

*E-mail: asalleo@stanford.edu.

Author Contributions

The manuscript was written through contributions of all authors. All authors have given approval to the final version of the manuscript.

Notes

The authors declare no competing financial interest.

ACKNOWLEDGMENTS

A.S. and C.C.W. gratefully acknowledge funding from the National Science Foundation (Career Award). K.V. and E.D.G. acknowledge financial support from NSF under Award DMR-1056199. Portions of this research were carried out at the Stanford Synchrotron Radiation Lightsource, a national user facility operated by Stanford University on behalf of the U.S. Department of Energy, Office of Basic Energy Sciences.

REFERENCES

(1) Chabinyc, M. L.; Wong, W. S.; Arias, A. C.; Ready, S.; Lujan, R. A.; Daniel, J. H.; Krusor, B.; Apte, R. B.; Salleo, A.; Street, R. A. *Proc. IEEE* **2005**, *93*, 1491−1499.

(2) Arias, A. C.; MacKenzie, D.; McCulloch, I.; Rivnay, J.; Salleo, A. *Chem. Rev.* **2010**, *110*, 3−24.

(3) Assadi, A.; Svensson, C.; Willander, M.; Iganas, O. *Appl. Phys. Lett.* **1988**, *53*, 195−197.

(4) McCullough, R. D.; Lowe, R. D.; Jayaraman, M.; Anderson, D. L. *J. Org. Chem.* **1993**, *58*, 904−912.

(5) Chen, T.-A.; Wu, X.; Rieke, R. D. *J. Am. Chem. Soc.* **1995**, *117*, 233−244.

(6) Bao, Z.; Dodabalapur, A.; Lovinger, A. J. *Appl. Phys. Lett.* **1996**, *69*, 4108−4110.

(7) Brown, G, P. J.; Friend, R. H.; Nielsen, M. M.; Bechgaard, K.; Langeveld-Voss, B. M. W.; Spiering, A. J. H.; Janssen, R. A. J.; Meijer, E. W.; Herwig, P.; de Leeuw, D. M. *Nature* **1999**, *401*, 685−688.

(8) Chang, J.-F.; Sirringhaus, H.; Giles, M.; Heeney, M.; McCulloch, I. *Phys. Rev. B* **2007**, *76*, 205204.

(9) Kline, R. J.; McGehee, M. D.; Kadnikova, E. N.; Liu, J.; Fréche, J. M. *J. Adv. Mater.* **2003**, *15*, 1519−1522.

(10) Goffri, S.; Müller, C.; Stingelin-Stutzmann, N.; Breiby, D. W.; Radano, C. P.; Andreasen, J. W.; Thompson, R.; Janssen, R. A. J.; Nielsen, M. M.; Smith, P.; Sirringhaus, H. *Nat. Mater.* **2006**, *5*, 950−956.

(11) Qiu, L.; Lee, W. H.; Wang, X., J. S.; Lim, J. A.; Kwak, D.; Lee, S.; Cho, K. *Adv. Mater.* **2009**, *21*, 1349−1353.

(12) Arias, A. C.; Endicott, F.; Street, R. A. *Adv. Mater.* **2006**, *18*, 2900−2904.

(13) Salleo, A.; Arias, A. C. *Adv. Mater.* **2007**, *19*, 3540−3543.

(14) Chabinyc, M. L.; Lu, J.-P.; Street, R. A. *J. Appl. Phys.* **2004**, *96*, 2063−2070.

(15) Wong, W. S.; Salleo, A. *Flexible Electronics: Materials and Applications*; Springer: New York, 2009; Chapter 6.

(16) Virkar, A.; Mannsfeld, S. C. B.; Bao, Z.; Stingelin, N. *Adv. Mater.* **2010**, *22*, 3857−3875.

(17) Paloheimo, J.; Kuivalainen, P.; Stubb, H.; Vuorimaa, E.; Yli-Lahti, P. *Appl. Phys. Lett.* **1990**, *56*, 1157−1159.

(18) Jimson, L. H.; Himmelberger, S.; Duong, D. T.; Rivnay, J.; Toney, M. F.; Salleo, A. *J. Pol. Phys. B.* in press.

(19) Baker, J. L.; Jimison, L. H.; Mannsfeld, S.; Volkman, S.; Yin, S.; Subramanian, V.; Salleo, A.; Alivisatos, A. P.; Toney, M. F. *Langmuir* **2010**, *26*, 9146−9151.

(20) Rivnay, J.; Salleo, A.; Mannsfeld, S. C. B.; Miller, C. E.; Toney, M. F. *Chem. Rev.* **2012**, *112*, 5488−5519.

(21) Rivnay, J.; Steyrleuthner, R.; Jimison, L. H.; Casadei, A.; Chen, Z.; Toney, M. F.; Facchetti, A.; Neher, D.; Salleo, A. *Macromolecules* **2011**, *44*, 5246−5255.

(22) Salleo, A. *Mater. Today* **2007**, *10*, 38−45.

(23) Kline, R. J.; McGehee, M. D.; Toney, M. F. *Nat. Mater.* **2006**, *5*, 222−228.

(24) Williamson, G. K.; Hall, W. H. *Acta Metall.* **1953**, *1*, 22−31.

(25) Warren, B. E. *X-Ray Diffraction*; Addison-Wesley: Reading, MA, 1969.

(26) Rivnay, J.; Noriega, R.; Kline, R. J.; Salleo, A.; Toney, M. F. *Phys. Rev. B* **2011**, *84*, 045203.